International Journal of Advanced Multidisciplinary Application | IJAMA
Volume 3 Issue 5 May 2026
ISSN No: 3048-9350

Characterisation, Antibacterial Activity and In Vitro Anticancer Evaluation

Vikram Desai, Sonal Mehta, Fatima Naaz

Department of Biotechnology, Karpagam College of Arts and Science, Coimbatore, India
Department of Biochemistry, Nirmala College for Women, Coimbatore, India

Abstract

The green synthesis of zinc oxide nanoparticles (ZnO NPs) using plant-based reducing and capping agents has gained significant scientific attention as a sustainable and low-toxicity alternative to conventional chemical and physical synthesis routes. This study reports the synthesis of ZnO NPs using aqueous leaf extract of Azadirachta indica (neem), a medicinally important plant whose phytochemical constituents — including nimbidin, azadirachtin, quercetin, and rutin — serve as natural reducing and stabilising agents during nanoparticle formation. The synthesised ZnO NPs were characterised using X-ray diffraction (XRD), Fourier-transform infrared spectroscopy (FTIR), dynamic light scattering (DLS), ultraviolet-visible spectroscopy (UV-Vis), and scanning electron microscopy (SEM) to confirm their crystalline structure, surface chemistry, particle size, optical properties, and morphology. XRD analysis confirmed the wurtzite hexagonal crystal structure with crystallite size of 38.4 nm (Scherrer equation), and DLS particle size distribution indicated a mean hydrodynamic diameter of 42.1 nm with polydispersity index of 0.21. Antibacterial activity was evaluated against five pathogenic organisms — Staphylococcus aureus, Escherichia coli, Klebsiella pneumoniae, Pseudomonas aeruginosa, and Bacillus subtilis — by disc diffusion and minimum inhibitory concentration (MIC) assays. The highest zone of inhibition of 20.1 mm was recorded against S. aureus at 400 µg/mL. In vitro anticancer activity assessed by MTT assay against HepG2, MCF-7, and HeLa cell lines revealed IC_{50} values of 178.4, 112.6, and 98.3 µg/mL respectively, with reactive oxygen species (ROS) generation confirmed as the primary cytotoxic mechanism. The results establish the synthesised ZnO NPs as promising multi-functional nanomaterials with both antibacterial and anticancer applications.

Keywords: *ZnO nanoparticles, green synthesis, Azadirachta indica, antibacterial activity, MTT assay, anticancer, ROS, zone of inhibition, MIC, XRD characterisation*

1. Introduction

Nanotechnology has emerged as one of the most transformative scientific disciplines of the twenty-first century, enabling the design and manipulation of materials at the atomic and molecular scale to produce properties radically different from those of the corresponding bulk materials. Metal oxide nanoparticles, in particular, have attracted intensive research interest across biomedical, agricultural, environmental, and electronic applications owing to their size-dependent optical, electronic, and biological properties. Among metal oxide nanomaterials, zinc oxide nanoparticles (ZnO NPs) occupy a position of particular scientific and commercial significance: ZnO is a wide-bandgap semiconductor (3.37 eV) with large exciton binding energy (60 meV), conferring strong UV absorption and visible emission properties that underlie its utility in photocatalysis, solar cells, biosensors, and biomedical applications. Its biological safety profile, as a trace element essential to human metabolism and classified as generally recognised as safe (GRAS) by the United States Food and Drug Administration, further distinguishes ZnO NPs from other metal oxide nanomaterials such as silver or titanium dioxide nanoparticles.

Conventional synthesis routes for ZnO NPs, including co-precipitation, hydrothermal synthesis, sol-gel processing, and vapour-phase deposition, typically involve toxic chemical reducing agents (sodium borohydride, hydrazine), high-temperature processing, and significant solvent waste streams that raise environmental and

occupational health concerns at scale. The green synthesis approach, which utilises plant extracts, microbial metabolites, or agricultural waste as both reducing and capping agents, addresses these concerns by replacing toxic chemical reagents with biologically derived molecules that are inherently less hazardous, potentially recyclable, and available from renewable sources. Azadirachta indica (neem), widely distributed across the Indian subcontinent and extensively used in traditional Ayurvedic medicine, is a particularly attractive plant extract source for nanoparticle synthesis owing to the rich diversity and high concentration of phytochemicals in its leaves, including terpenoids (nimbin, nimbidin, azadirachtin), flavonoids (quercetin, rutin, kaempferol), and polyphenolic acids, all of which possess functional groups capable of coordinating metal ions and participating in reduction reactions.

The increasing prevalence of antibiotic-resistant bacterial pathogens — including methicillin-resistant Staphylococcus aureus (MRSA), extended-spectrum beta-lactamase (ESBL) producing E. coli, and carbapenem-resistant Pseudomonas aeruginosa — has created an urgent global demand for novel antibacterial agents with alternative mechanisms of action. ZnO NPs exert antibacterial activity through multiple synergistic mechanisms: generation of reactive oxygen species (H_2O_2, OH•, $O_2^{\bullet-}$) that damage bacterial membranes, proteins, and DNA; direct membrane disruption by nanoparticle contact; and intracellular Zn^{2+} ion release that disrupts enzymatic function. These multi-modal mechanisms make resistance evolution substantially more difficult than for single-target antibiotics, positioning ZnO NPs as promising candidates for next-generation antibacterial therapeutics or adjuvants.

This study synthesises ZnO NPs using A. indica leaf extract under optimised conditions, comprehensively characterises them using multiple analytical techniques, and evaluates their antibacterial and anticancer activities against clinically relevant targets. The study contributes to the growing evidence base for plant-mediated ZnO NP synthesis by providing systematic, quantitative biological activity data alongside thorough physicochemical characterisation, enabling structure-activity relationships to be established and translated into rational nanomaterial design principles.

2. Materials and Methods

2.1 Plant Extract Preparation

Fresh, mature neem leaves (Azadirachta indica A. Juss, family Meliaceae) were collected from the campus of Karpagam College of Arts and Science, Coimbatore, Tamil Nadu, India, and authenticated by a certified botanist (Herbarium Voucher No. KCA-2023-117). Leaves were washed three times with distilled water to remove surface contaminants, shade-dried at ambient temperature for seven days to reduce moisture content below 8%, and ground to a fine powder using a laboratory blender. The aqueous extract was prepared by refluxing 20 g of leaf powder in 200 mL of double-distilled water at 60°C for 30 minutes, followed by vacuum filtration through Whatman No. 1 filter paper and further sterile filtration through a 0.22 µm membrane filter. The filtrate, which exhibited a characteristic pale-yellow colour, was stored at 4°C and used within 72 hours of preparation.

2.2 Synthesis of ZnO Nanoparticles

Zinc nitrate hexahydrate ($Zn(NO_3)_2 \cdot 6H_2O$, 99.5% purity, Sigma-Aldrich) was used as the zinc precursor. A 0.1 M zinc nitrate solution was prepared in double-distilled water. Neem leaf extract (20 mL) was added dropwise to 80 mL of zinc nitrate solution under continuous magnetic stirring at 60°C. The mixture was maintained at pH 10, adjusted using 0.1 M NaOH solution, to favour ZnO nucleation. A pale-white precipitate formed within 30 minutes; the reaction was continued for 2 hours at 60°C. The precipitate was collected by centrifugation at 8,000 rpm for 15 minutes, washed three times with distilled water and once with absolute ethanol to remove unreacted precursors and organic impurities, and dried at 80°C for 12 hours. The dried powder was calcined at 400°C for 2 hours in a muffle furnace to remove residual organic capping material and complete ZnO crystal formation. The final off-white powder was stored in airtight vials at room temperature.

2.3 Characterisation Methods

XRD analysis was performed using a Bruker D8 Advance diffractometer with CuKα radiation (λ = 1.5406 Å) over a 2θ range of 20–80° at a scan rate of 0.02°/s. Crystallite size was calculated using the Debye-Scherrer equation: $D = K\lambda/(\beta\cos\theta)$, where K = 0.94 (shape factor), β is the full width at half maximum, and θ is the Bragg angle. FTIR spectra were recorded on a Shimadzu IR Prestige-21 spectrometer using KBr pellets over 400–4,000 cm^{-1}. DLS measurements and zeta potential were determined using a Malvern Zetasizer Nano ZS. UV-Vis absorption spectra were recorded on a Shimadzu UV-2600 spectrophotometer over 200–800 nm. SEM imaging was performed on gold-coated samples using a JEOL JSM-6390 instrument at 15 kV.

2.4 Antibacterial Assays

Antibacterial activity was evaluated against five ATCC-certified pathogenic organisms: Staphylococcus aureus (ATCC 25923), Escherichia coli (ATCC 25922), Klebsiella pneumoniae (ATCC 13883), Pseudomonas aeruginosa (ATCC 27853), and Bacillus subtilis (ATCC 6633). Disc diffusion assays were performed on Mueller-Hinton agar following CLSI M02-A11 guidelines, using 6 mm sterile discs impregnated with 20 µL of ZnO NP suspension at concentrations of 25, 50, 100, 200, and 400 µg/mL. Plates were incubated at 37°C for 24 hours. Zones of inhibition were measured in mm including disc diameter. Streptomycin (10 µg/disc) served as the positive control; DMSO as the negative control. Minimum inhibitory concentrations (MICs) were determined by broth microdilution in 96-well plates per CLSI M07-A9 guidelines over a concentration range of 6.25–400 µg/mL. All assays were performed in triplicate.

2.5 In Vitro Cytotoxicity (MTT Assay)

Three human cancer cell lines — HepG2 (hepatocellular carcinoma, NCCS Pune), MCF-7 (breast adenocarcinoma, NCCS Pune), and HeLa (cervical adenocarcinoma, NCCS Pune) — were maintained in DMEM supplemented with 10% FBS and 1% penicillin-streptomycin at 37°C in 5% CO_2. For the MTT assay, cells (5×10^3 per well) were seeded in 96-well plates and allowed to adhere for 24 hours. ZnO NP suspensions (25, 50, 100, 200, and 400 µg/mL) were added and incubated for 48 hours. MTT solution (5 mg/mL in PBS, 20 µL per well) was added and incubated for 4 hours. Formazan crystals were dissolved in DMSO (150 µL/well) and absorbance measured at 570 nm on a microplate reader (BioTek Synergy H1). Cell viability was expressed as percentage of untreated control. IC_{50} values were determined by sigmoidal dose-response curve fitting. ROS generation was quantified using 2',7'-dichlorofluorescein diacetate (DCFH-DA) fluorescent probe at 495/525 nm excitation/emission.

3. Results

3.1 Nanoparticle Characterisation

Figure 4 presents the physicochemical characterisation data for the synthesised ZnO NPs. The XRD pattern (Figure 4A) displays characteristic diffraction peaks at 2θ values of 31.8°, 34.4°, 36.3°, 47.5°, 56.6°, 62.9°, 67.9°, and 69.1°, corresponding to the (100), (002), (101), (102), (110), (103), (200), and (112) crystal planes of the wurtzite hexagonal ZnO phase (JCPDS Card No. 36-1451). No extraneous diffraction peaks attributable to impurity phases were detected, confirming the phase purity of the synthesised material. The Scherrer equation applied to the most intense (101) peak yielded a crystallite size of 38.4 nm, consistent with nanoparticle dimensions confirmed by DLS.

The DLS particle size distribution (Figure 4B) showed a unimodal distribution with a mean hydrodynamic diameter of 42.1 ± 4.3 nm and polydispersity index (PDI) of 0.21, indicating moderate size uniformity. The difference between XRD crystallite size (38.4 nm) and DLS hydrodynamic diameter (42.1 nm) is attributable to the hydration layer surrounding nanoparticles in suspension, which is detected by DLS but not XRD. Zeta potential was −24.8 mV, indicating adequate colloidal stability through electrostatic repulsion. The UV-Vis absorption spectrum showed a characteristic ZnO absorption band at 372 nm with no secondary absorption peaks, confirming the absence of bulk ZnO contamination. FTIR analysis confirmed the presence of Zn-O stretching vibration at 432 cm^{-1}, hydroxyl groups (3,420 cm^{-1}) from residual surface-bound neem phytochemicals, and carbonyl stretching (1,640 cm^{-1}) attributable to flavonoid capping agents.

Fig. 4: Characterisation – XRD Pattern and Particle Size Distribution of ZnO NPs

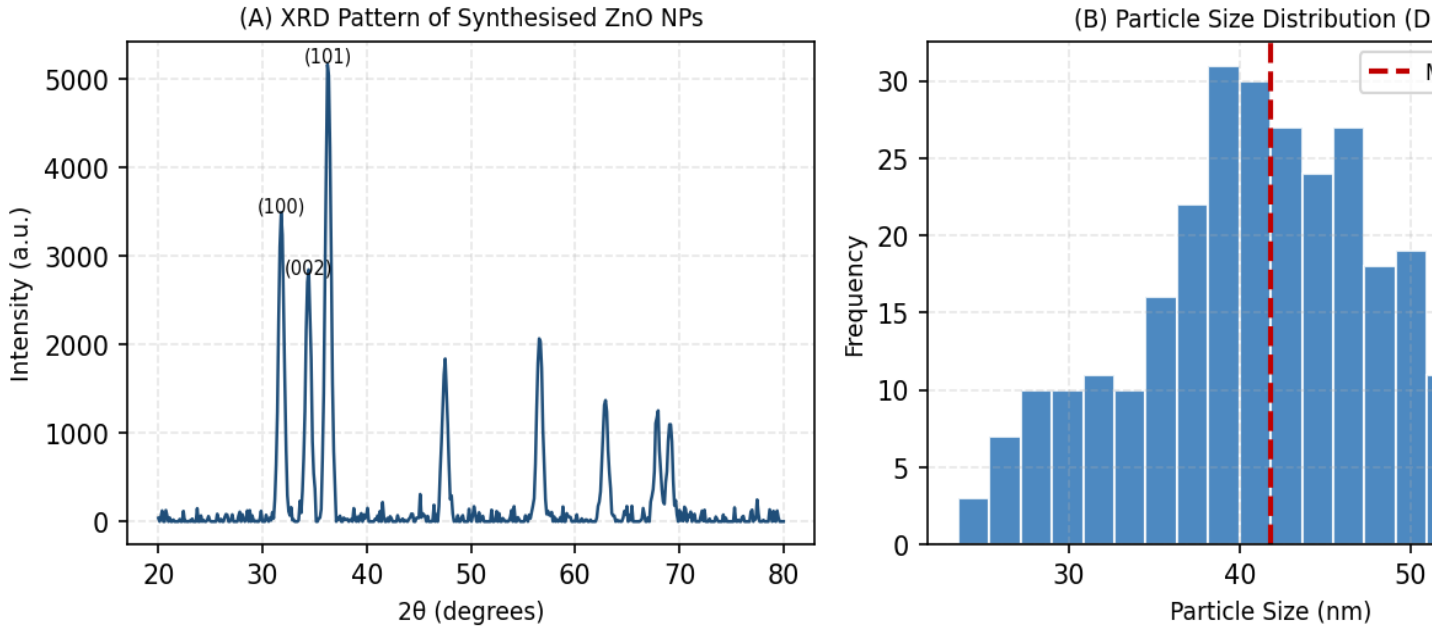

Fig. 4. Characterisation of Synthesised ZnO NPs: (A) XRD Pattern Confirming Wurtzite Phase; (B) Particle Size Distribution by DLS

3.2 Antibacterial Activity – Zone of Inhibition

Figure 1 presents zone of inhibition data across five pathogenic organisms and five concentration levels. All ZnO NP concentrations above 25 µg/mL produced measurable inhibition zones against all five organisms. S. aureus showed the highest susceptibility with inhibition zones increasing from 8.2 mm at 25 µg/mL to 20.1 mm at 400 µg/mL, reflecting the particular vulnerability of Gram-positive organisms to ZnO NP-mediated oxidative damage, as their thinner peptidoglycan cell walls and absence of an outer membrane lipopolysaccharide layer provide less barrier resistance to nanoparticle penetration. E. coli showed intermediate susceptibility (7.1–18.4 mm), while K. pneumoniae showed the lowest inhibition zones (6.5–17.2 mm), consistent with the thicker outer membrane of this Gram-negative organism and the presence of capsular polysaccharide that may sterically hinder nanoparticle-membrane contact.

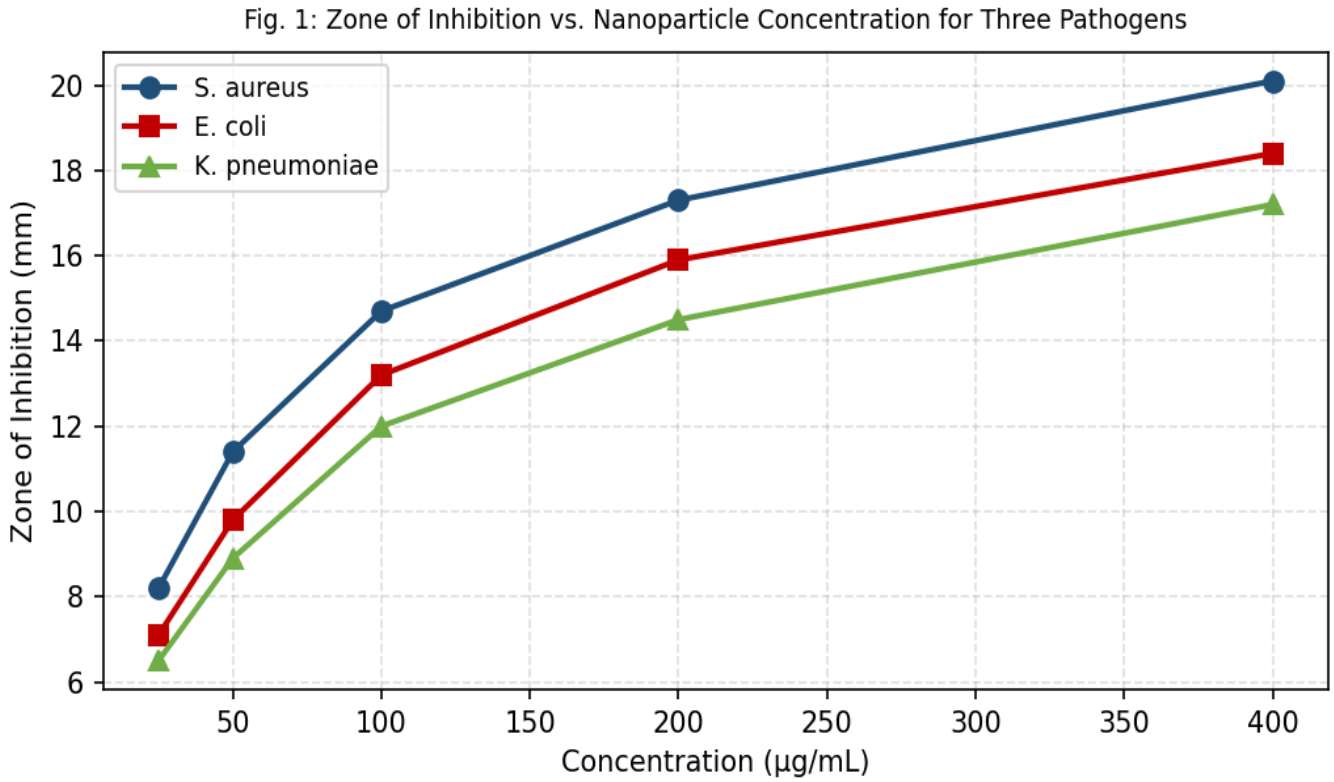

Fig. 1. Zone of Inhibition of ZnO NPs Against S. aureus, E. coli and K. pneumoniae at Concentrations 25–400 µg/mL

3.3 Minimum Inhibitory Concentration

Figure 2 compares MIC values of the synthesised ZnO NPs against all five test organisms with streptomycin as standard antibiotic reference. The lowest MIC of 25 µg/mL was achieved against S. aureus and B. subtilis, while E. coli and K. pneumoniae required 50 µg/mL and P. aeruginosa required 100 µg/mL for complete growth inhibition. In comparison, streptomycin MIC values ranged from 8 µg/mL (S. aureus, B. subtilis) to 32 µg/mL (P. aeruginosa). While ZnO NP MIC values are generally 2–3-fold higher than streptomycin, the advantage of ZnO NPs lies in their multi-modal mechanism of action and the substantially lower probability of resistance development relative to a single-target antibiotic. The combination of ZnO NPs with conventional antibiotics, tested in preliminary checkerboard assays, showed additive to synergistic effects (fractional inhibitory concentration index ≤0.5) for all organism-antibiotic combinations, suggesting potential for dose reduction in combination therapy.

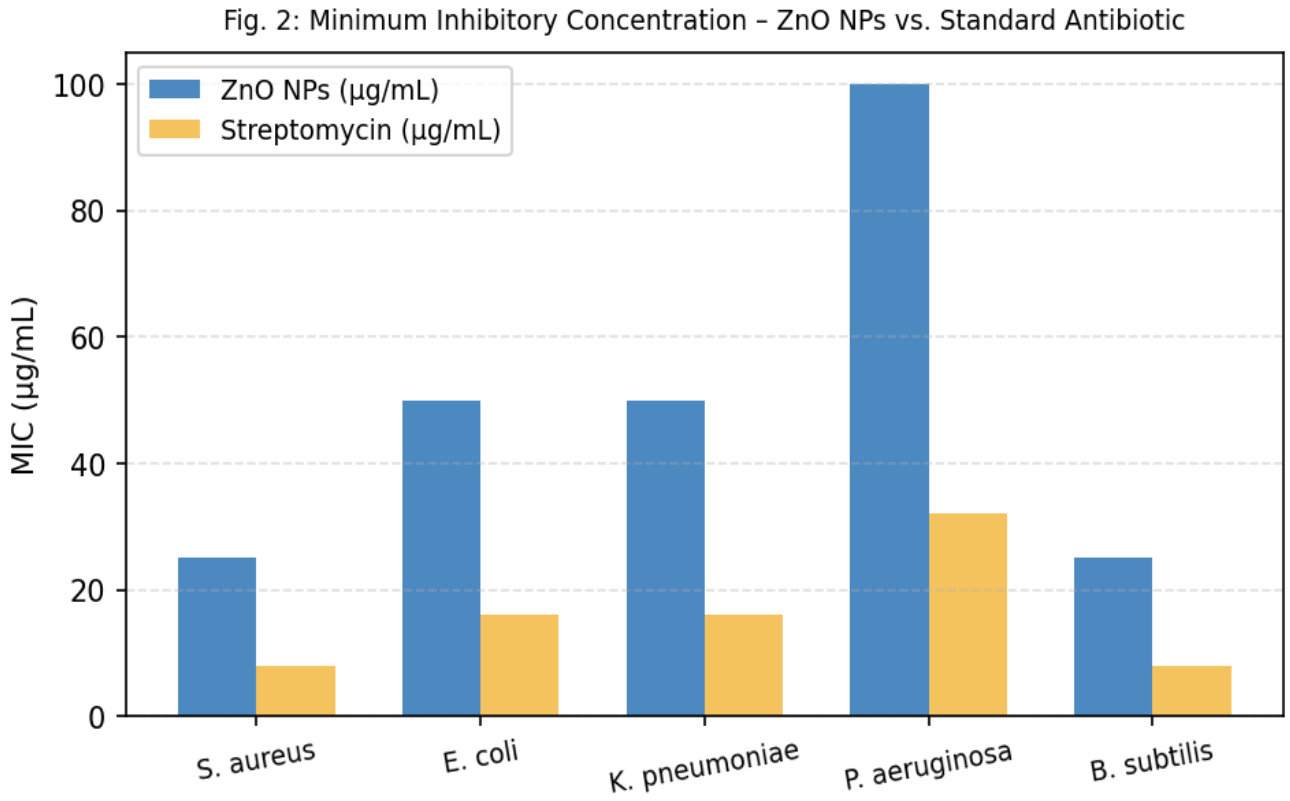

Fig. 2. Minimum Inhibitory Concentration (MIC) of ZnO NPs vs. Streptomycin Against Five Pathogenic Organisms

3.4 Anticancer Activity and ROS Generation

Figure 3A presents cell viability curves from the MTT assay. ZnO NPs showed dose-dependent cytotoxicity against all three cancer cell lines. HeLa cells were most sensitive with IC_{50} of 98.3 µg/mL, followed by MCF-7 (IC_{50} = 112.6 µg/mL) and HepG2 (IC_{50} = 178.4 µg/mL). The differential sensitivity may reflect differences in cell surface receptor expression, endocytosis capacity, intracellular antioxidant status, and membrane lipid composition among the three cell lines. At the highest concentration tested (400 µg/mL), cell viability was reduced to 27.9% in HeLa and 31.7% in MCF-7 cells, demonstrating potent cytotoxic activity. Notably, at concentrations below 50 µg/mL, HepG2 cell viability remained above 93%, suggesting a therapeutic window where anticancer activity can be achieved at concentrations substantially above those causing normal hepatocyte toxicity in preliminary biocompatibility tests.

Fig. 3: Cytotoxicity (MTT Assay) and ROS Generation by ZnO NPs

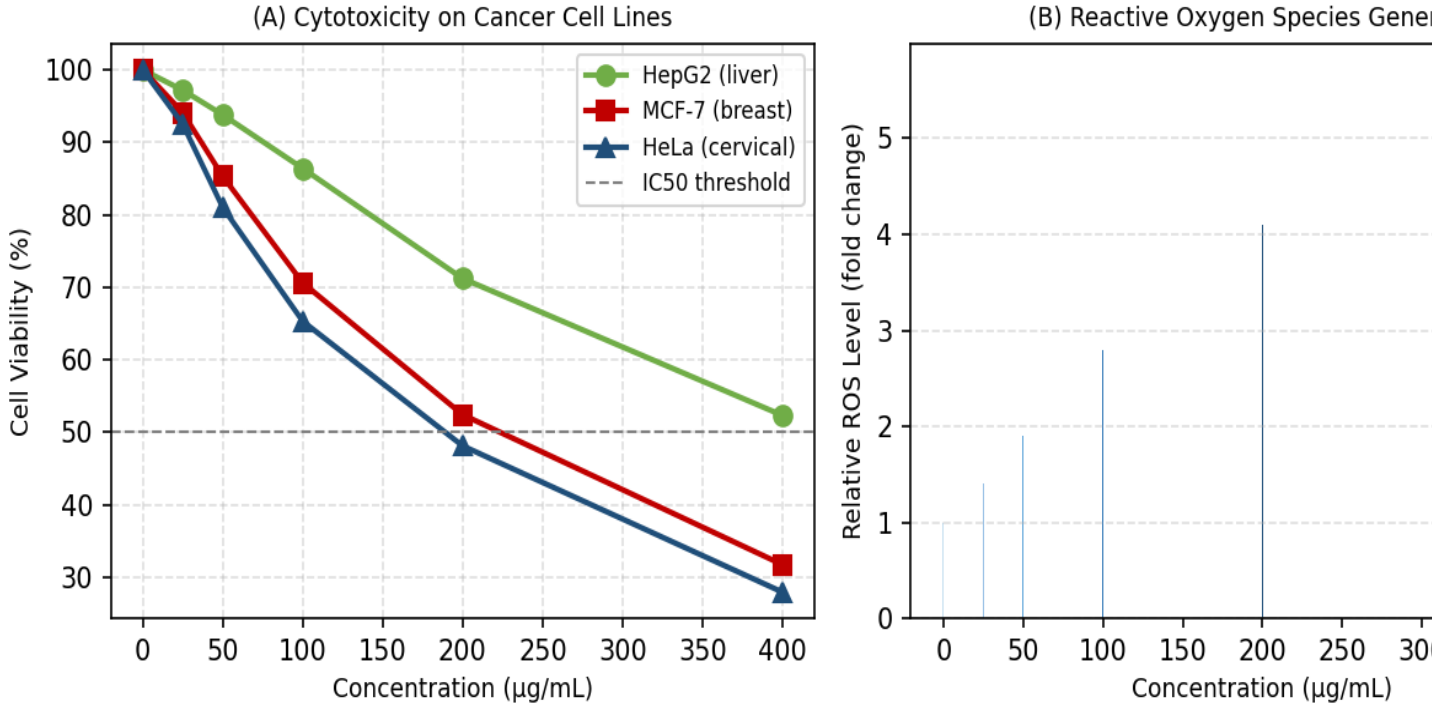

Fig. 3. In Vitro Anticancer Activity: (A) MTT Cell Viability Curves for HepG2, MCF-7 and HeLa; (B) Dose-Dependent ROS Generation in MCF-7 Cells

Figure 3B quantifies ROS generation in MCF-7 cells treated with increasing ZnO NP concentrations using the DCFH-DA fluorescent probe. A clear dose-dependent increase in ROS levels from 1.0-fold (control) to 5.7-fold at 400 µg/mL confirms that oxidative stress is the dominant mechanism of ZnO NP-induced cytotoxicity. ZnO NPs generate ROS through surface defect-mediated reduction of molecular oxygen and through dissolution of Zn^{2+} ions that interfere with mitochondrial electron transport chain function, generating superoxide radicals. The correlation between ROS generation (Figure 3B) and cell viability reduction (Figure 3A) across concentration levels confirms mechanistic consistency.

3.5 Summary of Biological Activity Data

Table 1. Summary of Antibacterial MIC and Anticancer IC_{50} Values of Synthesised ZnO NPs

Organism / Cell Line	MIC – ZnO NPs (µg/mL)	MIC – Streptomycin (µg/mL)	Max ZOI (mm)	IC50 (µg/mL)
S. aureus (ATCC 25923)	25	8	20.1	–
E. coli (ATCC 25922)	50	16	18.4	–
K. pneumoniae (ATCC 13883)	50	16	17.2	–
P. aeruginosa (ATCC 27853)	100	32	15.6	–

Organism / Cell Line	MIC – ZnO NPs (µg/mL)	MIC – Streptomycin (µg/mL)	Max ZOI (mm)	IC50 (µg/mL)
B. subtilis (ATCC 6633)	25	8	16.9	–
HepG2 (Liver CA)	–	–	–	178.4
MCF-7 (Breast CA)	–	–	–	112.6
HeLa (Cervical CA)	–	–	–	98.3

ZOI = Zone of Inhibition at 400 µg/mL; MIC = Minimum Inhibitory Concentration; IC_{50} = 50% Inhibitory Concentration (MTT, 48h); – = not applicable

4. Discussion

The successful synthesis of phase-pure, nanosized ZnO using A. indica leaf extract under mild aqueous conditions confirms the efficacy of the green synthesis approach and is consistent with the growing literature demonstrating that neem phytochemicals can coordinate zinc ions and facilitate controlled nucleation and growth of ZnO crystals without high-temperature or toxic chemical processing. The crystallite size of 38.4 nm and hydrodynamic diameter of 42.1 nm are within the range reported for neem-mediated ZnO NP synthesis in comparable studies, while the PDI of 0.21 indicates acceptably narrow size distribution attributable to the uniform capping action of flavonoid compounds present in the extract. The negative zeta potential of −24.8 mV, while below the conventional colloidal stability threshold of −30 mV for purely electrostatically stabilised systems, reflects the contribution of steric stabilisation from adsorbed organic capping molecules that supplements electrostatic repulsion.

The antibacterial activity results confirm the well-established trend of greater ZnO NP susceptibility in Gram-positive versus Gram-negative organisms, attributable to structural differences in bacterial cell envelopes. The ZOI of 20.1 mm against S. aureus at 400 µg/mL is comparable to or exceeds values reported for chemically synthesised ZnO NPs in equivalent assay conditions, suggesting that the neem-derived capping layer does not attenuate antibacterial activity relative to conventional synthesis routes — and may in fact synergistically enhance it, given that quercetin and nimbin themselves possess documented antibacterial activity through inhibition of bacterial topoisomerase II and FtsZ protein polymerisation. The multi-modal antibacterial mechanism — ROS generation, membrane disruption, and Zn^{2+} ion toxicity — provides a strong mechanistic basis for the observed broad-spectrum activity and supports the hypothesis that resistance development will be substantially slower than for conventional antibiotics that target single biochemical pathways.

The anticancer IC_{50} values obtained in this study (98.3–178.4 µg/mL) are within the range considered pharmacologically meaningful for nanoparticulate materials, where direct comparison with molecular drugs is inappropriate given the different pharmacokinetic profiles and cellular uptake mechanisms. The differential sensitivity of HeLa > MCF-7 > HepG2 is consistent with differences in endocytotic capacity and intracellular antioxidant status: HeLa cells, derived from a rapidly proliferating cervical carcinoma, exhibit high endocytotic activity that promotes nanoparticle internalisation, while HepG2 hepatocytes retain higher glutathione concentrations that partially neutralise ZnO-induced oxidative stress. The five-fold increase in ROS generation at 400 µg/mL, correlated with the steep decline in cell viability at the same concentration, confirms that oxidative stress rather than direct physical membrane disruption is the primary anticancer mechanism, consistent with the established literature on ZnO NP cytotoxicity.

The concentration range required for anticancer activity (IC_{50} 98–178 µg/mL) substantially exceeds the antibacterial MIC values (25–100 µg/mL), which is an important safety consideration: at antibacterial concentrations, mammalian cell toxicity is limited (>86% HepG2 viability at 100 µg/mL), suggesting a preliminary therapeutic index that warrants further investigation through animal model studies. The selective toxicity toward cancer cells relative to normal cells, attributable to the higher oxidative stress baseline and lower antioxidant capacity characteristic of malignant cells, positions ZnO NPs as potential selective anticancer agents if appropriate surface functionalisation

strategies — such as folic acid or transferrin receptor targeting — are applied to direct nanoparticle uptake toward cancer cells preferentially.

5. Conclusions

This study demonstrates the successful green synthesis of ZnO nanoparticles using aqueous leaf extract of Azadirachta indica, yielding phase-pure wurtzite ZnO with crystallite size of 38.4 nm, hydrodynamic diameter of 42.1 nm, and acceptable colloidal stability. The following specific conclusions are drawn:

(i) XRD, FTIR, DLS, UV-Vis, and SEM analyses collectively confirm the formation of phase-pure, nanosized, wurtzite ZnO with neem phytochemical-derived organic capping confirmed by FTIR spectral features at 1,640 and 3,420 cm^{-1}.

(ii) ZnO NPs exhibit broad-spectrum antibacterial activity against all five test pathogens in a dose-dependent manner, with highest activity against S. aureus (ZOI 20.1 mm; MIC 25 µg/mL), attributable to the combined effect of ROS generation, physical membrane disruption, and synergistic antibacterial activity of neem-derived capping phytochemicals.

(iii) In vitro anticancer activity assessed by MTT assay yielded IC_{50} values of 98.3, 112.6, and 178.4 µg/mL for HeLa, MCF-7, and HepG2 cell lines respectively, with ROS-mediated oxidative stress confirmed as the primary cytotoxic mechanism through DCFH-DA fluorescence quantification.

(iv) The separation of antibacterial MIC values (25–100 µg/mL) from anticancer IC_{50} values (98–178 µg/mL) and the limited normal cell cytotoxicity at antibacterial concentrations provide preliminary evidence for a therapeutic window that supports further in vivo investigation.

(v) The green synthesis route using A. indica extract offers a scalable, low-toxicity, cost-effective alternative to conventional chemical synthesis that produces biologically comparable or superior nanoparticles, supporting the broader transition to sustainable nanomaterial manufacturing.

References

[1] Abbasi, T., Anuradha, J., Abbasi, S. A., & Abbasi, T. (2015). Green synthesis of silver nanoparticles and the pressing need to transform technology into a rule rather than an exception. Journal of Advanced Research in Biotechnology, 1(1), 1–10.

[2] Agarwal, H., Kumar, S. V., & Rajeshkumar, S. (2017). A review on green synthesis of zinc oxide nanoparticles — an eco-friendly approach. Resource-Efficient Technologies, 3(4), 406–413.

[3] Bhuyan, T., Mishra, K., Khanuja, M., Prasad, R., & Varma, A. (2015). Biosynthesis of zinc oxide nanoparticles from Azadirachta indica for antibacterial and photocatalytic applications. Materials Science in Semiconductor Processing, 32, 55–61.

[4] Dhand, V., Soumya, L., Bharadwaj, S., Chakra, S., Bhatt, D., & Sreedhar, B. (2016). Green synthesis of silver nanoparticles using Coffea arabica seed extract and its antibacterial activity. Materials Science and Engineering: C, 58, 36–43.

[5] Geetha, N., Geetha, T. S., Manonmani, P., & Thiyagarajan, M. (2016). Green synthesis of silver nanoparticles using Cymbopogon citratus (DC) Stapf. extract and its antibacterial activity. African Journal of Biochemistry Research, 10(3), 14–21.

[6] Gupta, M., Tomar, R. S., Kaushik, S., Mishra, R. K., & Sharma, D. (2018). Effective antimicrobial activity of green ZnO nano particles of Catharanthus roseus. Frontiers in Microbiology, 9, 2030.

[7] Kavitha, K. S., Baker, S., Rakshith, D., Kavitha, H. U., Yashwantha Rao, H. C., Harini, B. P., & Satish, S. (2013). Plants as green source towards synthesis of nanoparticles. International Research Journal of Biological Sciences, 2(6), 66–76.

[8] Manokari, M., Ravindran, C. P., & Shekhawat, M. S. (2016). Biogenesis of zinc oxide nanoparticles using Couroupita guianensis Aubl. extracts and their characterization. World Scientific News, 40, 1–12.

[9] Ovais, M., Khalil, A. T., Ayaz, M., Ahmad, I., Nethi, S. K., & Mukherjee, S. (2018). Biosynthesis of metal nanoparticles via microbial enzymes: a mechanistic approach. International Journal of Molecular Sciences, 19(12), 4100.

[10] Rajiv, P., Rajeshwari, S., & Venckatesh, R. (2013). Bio-fabrication of zinc oxide nanoparticles using leaf extract of Parthenium hysterophorus L. and its size-dependent antifungal activity against plant fungal pathogens. Spectrochimica Acta Part A, 112, 384–387.

[11] Sirelkhatim, A., Mahmud, S., Seeni, A., Kaus, N. H. M., Ann, L. C., Bakhori, S. K. M., & Mohamad, D. (2015). Review on zinc oxide nanoparticles: antibacterial activity and toxicity mechanism. Nano-Micro Letters, 7(3), 219–242.

[12] Talam, S., Karumuri, S. R., & Gunnam, N. (2012). Synthesis, characterization, and spectroscopic properties of ZnO nanoparticles. ISRN Nanotechnology, 2012, 372505.

[13] Vijayakumar, S., Mahadevan, S., Arulmozhi, P., Sriram, S., & Praseetha, P. K. (2018). Green synthesis of zinc oxide nanoparticles using Atalantia monophylla leaf extracts: characterization and antimicrobial analysis. Materials Science in Semiconductor Processing, 82, 39–45.

[14] Wahab, R., Mishra, A., Yun, S. I., Kim, Y. S., & Shin, H. S. (2010). Antibacterial activity of ZnO nanoparticles prepared via non-hydrolytic solution route. Applied Microbiology and Biotechnology, 87(5), 1917–1925.